

## STABILITY ANALYSIS FOR MAXIMUM PRINCIPLE PRESERVING EXPLICIT ISOTROPIC SCHEMES OF THE ALLEN-CAHN EQUATION\*

Jyoti

*The Institute of Basic Science, Korea University, Seoul 02841, Republic of Korea*

*Email: jyoti@korea.ac.kr*

Seokjun Ham, Soobin Kwak, Youngjin Hwang, Seungyoon Kang and Junseok Kim<sup>1)</sup>

*Department of Mathematics, Korea University, Seoul 02841, Republic of Korea*

*Emails: seokjun@korea.ac.kr, soobin23@korea.ac.kr, youngjin\_hwang@korea.ac.kr,*

*heroe2401@korea.ac.kr, cfdkim@korea.ac.kr*

### Abstract

In practical applications, the Allen-Cahn (AC) equation is commonly used to model microstructure evolutions, including alloy solidification, crystal growth, fingerprint image restoration, and image segmentation. However, when we discretize the AC equation with a conventional finite difference scheme, the directional bias in error terms introduces anisotropy into the numerical results, affecting interface dynamics. To address this issue, we use two- and three-dimensional isotropic finite difference schemes to solve the AC equation. Stability of the proposed algorithm is verified by deriving the time step constraints in both 2D and 3D domains. To demonstrate the sharp estimation of the stability constraints, we conducted several numerical experiments and found the maximum principle is guaranteed under the analyzed time-step constraint.

*Mathematics subject classification:* 65M06, 65M12.

*Key words:* Allen-Cahn equation, Finite difference method, Isotropic discretization, Discrete Laplacian operator.

### 1. Introduction

In this paper, we present the stability analysis of fully explicit isotropic finite difference numerical schemes that solve the Allen-Cahn equation [1]

$$\frac{\partial \psi(\mathbf{x}, t)}{\partial t} = -\frac{F'(\psi(\mathbf{x}, t))}{\epsilon^2} + \Delta\psi(\mathbf{x}, t), \quad \mathbf{x} \in \Omega, \quad t > 0, \quad (1.1)$$

where  $\Omega$  is a domain that belongs to  $\mathbb{R}^d$  ( $d = 2, 3$ ),  $F(\psi)$  represents the energy potential, and  $\epsilon$  denotes the interface thickness parameter. In this paper, the zero Neumann boundary condition is applied as  $\mathbf{n} \cdot \nabla\psi(\mathbf{x}, t) = 0$  on  $\partial\Omega$ . Here,  $\mathbf{n}$  is normal to  $\partial\Omega$ . The AC equation is derived as the  $L^2$ -gradient flow of the following total energy functional:

$$\mathcal{E}(\psi) = \int_{\Omega} \left( \frac{F(\psi)}{\epsilon^2} + \frac{1}{2} |\nabla\psi|^2 \right) d\mathbf{x}, \quad (1.2)$$

where  $F(\psi) = 0.25(\psi^2 - 1)^2$  is the bulk energy potential as illustrated in Fig. 1.1.

\* Received May 31, 2024 / Revised version received August 22, 2024 / Accepted April 3, 2025 /

Published online June 4, 2025 /

<sup>1)</sup> Corresponding Author

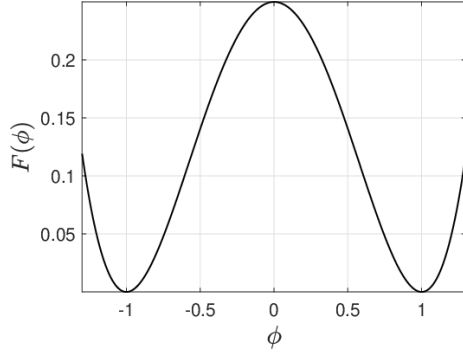


Fig. 1.1. Polynomial double-well potential energy.

In literature [4,18,36], phase-field modeling has proven to be a reliable approach for conducting quantitative assessments of microstructure evolution such as alloy solidification [4], dendritic growth, fingerprint image restoration [31], image segmentation [27], and many more. However, it is impossible to derive an analytical solution of the nonlinear AC equation with arbitrary initial conditions. As a result, numerical methods such as finite volume method (FVM) [29], finite element method (FEM) [30], spectral methods [10], and finite difference method (FDM) [20] become essential to approximate the solutions of the AC equation.

There are numerous practical applications of phase-field equation including image segmentation, image inpainting [40], crystal growth problems, topology optimization [44], shape transformation [21], transport network optimization [43], additive manufacturing [24], surfactant system [19], nucleation and crystallization [42]. In these applications phase field equations like the AC equation can be used to study the minimal hypersurfaces. Applications of the AC equation, such as the stochastic AC equation is widely studied by many researchers [35]. There is a study by Lee [26] in which a numerical method that constructs minimal hypersurfaces that was used. The author introduced two examples of minimal surfaces such as, catenoid and Scherk's. However, to support the strength of the proposed method positive definite property and boundedness property was proved theoretically. Also, in the study by [16] a practical adaptive FDM is presented for solving the AC equation in 2D space. The proposed method is applicable to simulate thin capillary driven films, wobbling bubble, and tumor growth. However, it is noticeable that for such kind of practical applications, when employing conventional finite-difference techniques to discretize the AC equation, it introduces a form of anisotropy into the numerical scheme caused by the directional bias of error terms [18]. This anisotropy affects the dynamics of the interface when discretizing the equations on a uniform grid, grid points are organized on a square lattice in 2D [25] or a cubic lattice in 3D [2], respectively. Batangouna [5] proposed a time semidiscretization method using backward Euler scheme to solve Ginzburg-Landau equation, which reduced the AC equation with specific conditions. It was found that their method was convergent and applicable in various fractal dimensions. Additionally, asymptotic behavior and error estimation are of great importance. The works of Tang and Yang [39], as well as Shen *et al.* [37], are good examples of theoretical results that support the proposed numerical methods.

An explicit isotropic FDM is an efficient method of the AC equation. The incorporation of isotropic discretization in 2D and 3D Laplacian operator will enable us to accurately calculate the discrepancies between the numerical approximations and the exact analytical solutions.

Furthermore, when adopting an adaptive mesh, the algorithm shows high efficiency. However, for accuracy, an explicit FDM needs some time step constraint. Additionally, it is important that the computational solutions to the AC equation preserve the physical properties of the AC equation. Liu *et al.* [32] proposed a numerical method of the conservative AC equation that preserves the energy dissipation, mass conservation, and maximum principle simultaneously at the fully discrete level. The given numerical experiments substantiate the theoretical analysis on the convergence and properties and of the AC equation. Similar study is given in Gong *et al.* [11] where two maximum bound property preserving iteration technique are proposed. The authors implemented numerical experiments for the AC model to verify the theoretical investigations and highlight the effectiveness in long time simulations. Chu *et al.* [7] developed a method for solving the AC equation based on the second-order Crank-Nicolson method. The authors applied second order central difference method for discretization. The unconditional stability and maximum principle is proven for the proposed method. Numerical experiments verified the theoretical results. Tang and Yang [39] studied the maximum principle and the discrete energy stability of the implicit-explicit scheme for the AC equation. They provided theoretical framework is independent of dimensions and only requires a simple restriction, time step size under 0.5. Numerical tests using a random initial condition show good agreement with the theoretical results given in the paper. Shen *et al.* [37] extended the study initiated by Tang and Yang by formulating maximum-principle-preserving numerical schemes for the generalized AC equation. The numerical maximum principle is considered using semi-implicit discretization and a central finite difference scheme applied to the diffusion term. For the advection term, the upwind scheme is applied. Numerical experiments verified the theoretical results. Gu *et al.* [12] presented a Saul'yev based numerical scheme for the AC equation that preserves energy stability and maximum bound principle. Both theoretical analysis and numerical experiments are conducted to verify the physical properties of the AC equation. Suzuki *et al.* [38] also highlighted the importance of the stability when considering the AC equation. Theoretical background for the stability of the proposed method is given in the paper. Chen *et al.* [6] coupled the AC equation with the incompressible Navier-Stokes equation. Energy stability of both the scheme and the fully discrete scheme is proven in the paper. Numerical results supported the applicability of the proposed method.

Therefore, the core objective of this work is to propose stability analysis of fully explicit isotropic FDMs for numerically solving the AC equation so that we can use time steps which guarantee the maximum principle and stability.

The structure of this paper is as follows. The numerical solution algorithms are given in Section 2. Some computational tests are presented in Section 3. Conclusion is given in Section 4.

## 2. Numerical Solution Algorithms

Isotropic discretization plays an essential role in maintaining the inherent symmetry of the underlying continuous problem; in situations where the physical phenomena being modeled exhibit symmetry along distinct directions, the adoption of isotropic discretization becomes important and ensures that the numerical solution accurately preserves and shows this symmetry throughout the computational process. The isotropic discretization is important not only in symmetric cases but also in non-symmetric cases because it helps accurately preserving the structural characteristics of the problems under consideration.

We introduce fully explicit FDMs for the AC equation and begin by examining the equation in a 2D domain  $\Omega = (L_x, R_x) \times (L_y, R_y)$  with number of spatial grid points  $N_x$  and  $N_y$ . A uniform spatial grid size

$$h = \frac{R_x - L_x}{N_x} = \frac{R_y - L_y}{N_y}$$

is applied. The discretized domain is defined as

$$\Omega_h = \{(x_p, y_q) \mid x_p = L_x + (p - 0.5)h, y_q = L_y + (q - 0.5)h, p = 1, 2, \dots, N_x, q = 1, 2, \dots, N_y\}.$$

On the computational domain,  $\psi(x_p, y_q, n\Delta t)$  is approximated by  $\psi_{pq}^n$  for  $n = 1, 2, \dots, N_t$ . Here,  $T$  is final time,  $N_t$  is number of time steps, and  $\Delta t = T/N_t$  is time step. We define the discrete Laplacian operator with a 9-point isotropic stencil in 2D as follows:

$$\begin{aligned} \Delta\psi_{pq} = \frac{1}{6h^2} & [4(\psi_{p-1,q} + \psi_{p+1,q} + \psi_{p,q-1} + \psi_{p,q+1}) \\ & + \psi_{p-1,q+1} + \psi_{p-1,q-1} + \psi_{p+1,q-1} + \psi_{p+1,q+1} - 20\psi_{pq}]. \end{aligned}$$

At the 2D computational domain, for  $p = 1, 2, \dots, N_x, q = 1, 2, \dots, N_y$ , the zero Neumann boundary condition is applied as follows:

$$\psi_{0,q} = \psi_{1,q}, \quad \psi_{N_x+1,q} = \psi_{N_x,q}, \quad \psi_{p,0} = \psi_{p,1}, \quad \psi_{p,N_y+1} = \psi_{p,N_y}.$$

We use the explicit Euler method for temporal discretization as follows:

$$\begin{aligned} & \frac{\psi_{pq}^{n+1} - \psi_{pq}^n}{\Delta t} + \mathcal{O}(\Delta t) \\ &= -\frac{(\psi_{pq}^n)^3 - \psi_{pq}^n}{\epsilon^2} + \Delta\psi_{pq}^n + \mathcal{O}(h^2) \\ &= -\frac{(\psi_{pq}^n)^3 - \psi_{pq}^n}{\epsilon^2} \\ & \quad + \frac{1}{6h^2} [4(\psi_{p-1,q}^n + \psi_{p+1,q}^n + \psi_{p,q-1}^n + \psi_{p,q+1}^n) \\ & \quad + \psi_{p-1,q+1}^n + \psi_{p-1,q-1}^n + \psi_{p+1,q-1}^n + \psi_{p+1,q+1}^n - 20\psi_{pq}^n] + \mathcal{O}(h^2). \end{aligned} \quad (2.1)$$

Next, we define the AC equation in the three-dimensional (3D) domain

$$\Omega = (L_x, R_x) \times (L_y, R_y) \times (L_z, R_z)$$

with number of spatial grid points  $N_x, N_y$  and  $N_z$ . A uniform spatial grid size

$$h = \frac{R_x - L_x}{N_x} = \frac{R_y - L_y}{N_y} = \frac{R_z - L_z}{N_z}$$

is applied. Let us consider the discretized domain as

$$\begin{aligned} \Omega_h = \{(x_p, y_q, z_r) \mid x_p &= L_x + (i - 0.5)h, y_q = L_y + (j - 0.5)h, z_r = L_z + (k - 0.5)h, \\ & p = 1, 2, \dots, N_x, q = 1, 2, \dots, N_y, r = 1, 2, \dots, N_z\}. \end{aligned}$$

On the discretized domain,  $\psi(x_p, y_q, z_r, n\Delta t)$  is approximated as  $\psi_{pqr}^n$  for  $n = 1, 2, \dots, N_t$  where  $\Delta t = T/N_t$  denotes time step size, with  $N_t$  representing the total number of time steps and  $T$

the final time. The isotropic discrete Laplacian operator is defined with a 27-point isotropic stencil [28] in 3D as follows:

$$\begin{aligned}
(\Delta_\beta \psi)_{pqr} = & \frac{1}{h^2(\alpha + 4\beta + 4\gamma)} (\alpha(\psi_{p+1,qr} + \psi_{p-1,qr} + \psi_{p,q+1,r} + \psi_{p,q-1,r} + \psi_{pq,r+1} + \psi_{pq,r-1}) \\
& + \beta(\psi_{p+1,q,r-1} + \psi_{p-1,q,r-1} + \psi_{p,q+1,r-1} + \psi_{p,q-1,r-1} \\
& + \psi_{p+1,q+1,r} + \psi_{p-1,q+1,r} \\
& + \psi_{p+1,q-1,r} + \psi_{p-1,q-1,r} + \psi_{p+1,q,r+1} \\
& + \psi_{p-1,q,r+1} + \psi_{p,q+1,r+1} + \psi_{p,q-1,r+1}) \\
& + \gamma(\psi_{p+1,q+1,r-1} + \psi_{p-1,q+1,r-1} + \psi_{p+1,q-1,r-1} + \psi_{p-1,q-1,r-1} \\
& + \psi_{p+1,q+1,r+1} + \psi_{p-1,q+1,r+1} \\
& + \psi_{p+1,q-1,r+1} + \psi_{p-1,q-1,r+1}) - (6\alpha + 12\beta + 8\gamma)\psi_{pqr}),
\end{aligned}$$

where  $\alpha, \beta$ , and  $\gamma$  are non-negative values and we can assume that  $\alpha + \beta + \gamma = 1$  without losing generality. Here, we can take  $\alpha = 2/3, \beta = 1/3$ , and  $\gamma = 0$  to obtain the 19-point stencil discrete Laplacian operator as follows:

$$\begin{aligned}
(\Delta_{\frac{1}{3}} \psi)_{pqr} = & \frac{1}{6h^2} (2(\psi_{p+1,qr} + \psi_{p-1,qr} + \psi_{p,q+1,r} + \psi_{p,q-1,r} + \psi_{pq,r+1} + \psi_{pq,r-1}) \\
& + \psi_{p+1,q,r-1} + \psi_{p-1,q,r-1} + \psi_{p,q+1,r-1} + \psi_{p,q-1,r-1} \\
& + \psi_{p+1,q+1,r} + \psi_{p-1,q+1,r} + \psi_{p+1,q-1,r} + \psi_{p-1,q-1,r} \\
& + \psi_{p+1,q,r+1} + \psi_{p-1,q,r+1} + \psi_{p,q+1,r+1} + \psi_{p,q-1,r+1} - 24\psi_{pqr}).
\end{aligned}$$

For the 3D numerical domain, for  $p = 1, 2, \dots, N_x, q = 1, 2, \dots, N_y, r = 1, 2, \dots, N_z$ , the homogeneous Neumann boundary condition is applied as follows:

$$\begin{aligned}
\psi_{0,qr} &= \psi_{1,qr}, & \psi_{N_x+1,qr} &= \psi_{N_x,qr}, & \psi_{p,0,r} &= \psi_{p,1,r}, \\
\psi_{p,N_y+1,r} &= \psi_{p,N_y,r}, & \psi_{pq,0} &= \psi_{pq,1}, & \psi_{pq,N_z+1} &= \psi_{pq,N_z}.
\end{aligned}$$

We use the explicit Euler method for time. Therefore, we have following equation using the 27-point stencil discrete Laplacian operator:

$$\begin{aligned}
& \frac{\psi_{pqr}^{n+1} - \psi_{pqr}^n}{\Delta t} + \mathcal{O}(\Delta t) \\
& = -\frac{(\psi_{pqr}^n)^3 - \psi_{pqr}^n}{\epsilon^2} + \Delta \psi_{pqr}^n + \mathcal{O}(h^2) \\
& = -\frac{(\psi_{pqr}^n)^3 - \psi_{pqr}^n}{\epsilon^2} \\
& \quad + \frac{1}{h^2(\alpha + 4\beta + 4\gamma)} (\alpha(\psi_{p+1,qr}^n + \psi_{p-1,qr}^n + \psi_{p,q+1,r}^n + \psi_{p,q-1,r}^n + \psi_{pq,r+1}^n + \psi_{pq,r-1}^n) \\
& \quad + \beta(\psi_{p+1,q,r-1}^n + \psi_{p-1,q,r-1}^n + \psi_{p,q+1,r-1}^n + \psi_{p,q-1,r-1}^n + \psi_{p+1,q+1,r}^n \\
& \quad + \psi_{p-1,q+1,r}^n + \psi_{p+1,q-1,r}^n + \psi_{p-1,q-1,r}^n + \psi_{p+1,q,r+1}^n + \psi_{p-1,q,r+1}^n \\
& \quad + \psi_{p,q+1,r+1}^n + \psi_{p,q-1,r+1}^n) \\
& \quad + \gamma(\psi_{p+1,q+1,r-1}^n + \psi_{p-1,q+1,r-1}^n + \psi_{p+1,q-1,r-1}^n + \psi_{p-1,q-1,r-1}^n \\
& \quad + \psi_{p+1,q+1,r+1}^n + \psi_{p-1,q+1,r+1}^n + \psi_{p+1,q-1,r+1}^n + \psi_{p-1,q-1,r+1}^n) \\
& \quad - (6\alpha + 12\beta + 8\gamma)\psi_{pqr}^n) + \mathcal{O}(h^2). \tag{2.2}
\end{aligned}$$

Hence, we can obtain the following numerical solution using the 19-point stencil discrete Laplacian operator with  $\alpha = 1/3$ ,  $\beta = 2/3$ , and  $\gamma = 0$ :

$$\begin{aligned} & \frac{\psi_{pqr}^{n+1} - \psi_{pqr}^n}{\Delta t} + \mathcal{O}(\Delta t) \\ &= -\frac{(\psi_{pqr}^n)^3 - \psi_{pqr}^n}{\epsilon^2} \\ &\quad + \frac{1}{6h^2} (2(\psi_{p+1,qr} + \psi_{p-1,qr} + \psi_{p,q+1,r} + \psi_{p,q-1,r} + \psi_{pq,r+1} + \psi_{pq,r-1}) \\ &\quad + \psi_{p+1,q,r-1} + \psi_{p-1,q,r-1} + \psi_{p,q+1,r-1} + \psi_{p,q-1,r-1} \\ &\quad + \psi_{p+1,q+1,r} + \psi_{p-1,q+1,r} + \psi_{p+1,q-1,r} + \psi_{p-1,q-1,r} \\ &\quad + \psi_{p+1,q,r+1} + \psi_{p-1,q,r+1} + \psi_{p,q+1,r+1} + \psi_{p,q-1,r+1} - 24\psi_{pqr}) + \mathcal{O}(h^2). \end{aligned}$$

The following two theorems confirm the maximum principle of the scheme with time step restrictions for a 9-point stencil in 2D and 19- and 27-point stencils in 3D.

**Theorem 2.1.** Suppose that  $\max_{1 \leq p \leq N_x, 1 \leq q \leq N_y} |\psi_{pq}^0| \leq 1$ . Then, numerical solutions of the isotropic scheme (2.1) is bounded, i.e.

$$|\psi_{pq}^{n+1}| \leq 1, \quad \text{for } 1 \leq p \leq N_x, \quad 1 \leq q \leq N_y, \quad n \geq 0, \quad (2.3)$$

if  $\Delta t$  satisfies

$$\Delta t \leq \frac{3\epsilon^2 h^2}{6h^2 + 10\epsilon^2}. \quad (2.4)$$

*Proof.* The explicit isotropic method for the 2D AC equation (2.1) is given as

$$\begin{aligned} \psi_{pq}^{n+1} &= \psi_{pq}^n + \Delta t \left\{ \frac{\psi_{pq}^n - (\psi_{pq}^n)^3}{\epsilon^2} \right. \\ &\quad + \frac{1}{6h^2} [4(\psi_{p-1,q}^n + \psi_{p+1,q}^n + \psi_{p,q-1}^n + \psi_{p,q+1}^n) \\ &\quad \left. + \psi_{p-1,q+1}^n + \psi_{p-1,q-1}^n + \psi_{p+1,q-1}^n + \psi_{p+1,q+1}^n - 20\psi_{pq}^n] \right\}. \quad (2.5) \end{aligned}$$

**Case 1.**  $\psi_{pq}^n = 1$ . Eq. (2.5) is given as

$$\begin{aligned} \psi_{pq}^{n+1} &= 1 + \frac{\Delta t}{6h^2} [4(\psi_{p-1,q}^n + \psi_{p+1,q}^n + \psi_{p,q-1}^n + \psi_{p,q+1}^n) \\ &\quad + \psi_{p-1,q+1}^n + \psi_{p-1,q-1}^n + \psi_{p+1,q-1}^n + \psi_{p+1,q+1}^n - 20] \leq 1, \quad (2.6) \end{aligned}$$

because

$$4(\psi_{p-1,q}^n + \psi_{p+1,q}^n + \psi_{p,q-1}^n + \psi_{p,q+1}^n) + \psi_{p-1,q+1}^n + \psi_{p-1,q-1}^n + \psi_{p+1,q-1}^n + \psi_{p+1,q+1}^n - 20 \leq 0.$$

If  $\Delta t \leq 3h^2/10$  holds,  $\psi_{pq}^{n+1} \geq -1$  and therefore  $|\psi_{pq}^{n+1}| \leq 1$  is satisfied.

**Case 2.**  $0 \leq \psi_{pq}^n < 1$ . In Eq. (2.5), we consider the following two conditions of  $\Delta t$ : condition for  $\psi_{pq}^{n+1} \leq 1$  and  $\psi_{pq}^{n+1} \geq -1$ . For the first case, we apply  $\psi_{p-1,q}^n, \psi_{p+1,q}^n, \psi_{p,q-1}^n, \psi_{p,q+1}^n, \psi_{p-1,q+1}^n, \psi_{p-1,q-1}^n, \psi_{p+1,q-1}^n, \psi_{p+1,q+1}^n \leq 1$  to Eq. (2.5). Therefore the goal is to find  $\Delta t$  that satisfies the following inequality:

$$\psi_{pq}^{n+1} \leq \psi_{pq}^n + \Delta t \left[ \frac{\psi_{pq}^n - (\psi_{pq}^n)^3}{\epsilon^2} + \frac{1}{3h^2} (10 - 10\psi_{pq}^n) \right] \leq 1. \quad (2.7)$$

Eq. (2.7) can be rewritten and simplified by dividing both sides by  $(1 - \psi_{pq}^n) > 0$

$$\begin{aligned}\Delta t(1 - \psi_{pq}^n) \left( \frac{\psi_{pq}^n(1 + \psi_{pq}^n)}{\epsilon^2} + \frac{10}{3h^2} \right) &\leq 1 - \psi_{pq}^n, \\ \Delta t \left( \frac{\psi_{pq}^n(1 + \psi_{pq}^n)}{\epsilon^2} + \frac{10}{3h^2} \right) &\leq 1.\end{aligned}$$

Hence, we obtain the following  $\Delta t$  condition satisfying  $\psi_{pq}^{n+1} \leq 1$ :

$$\Delta t \leq \frac{3\epsilon^2 h^2}{3h^2 \psi_{pq}^n (1 + \psi_{pq}^n) + 10\epsilon^2}.$$

Because  $0 < \psi_{pq}^n(1 + \psi_{pq}^n) < 2$ , we obtain the condition satisfying  $|\psi_{pq}^{n+1}| \leq 1$  as follows:

$$\Delta t \leq \frac{3\epsilon^2 h^2}{6h^2 + 10\epsilon^2}.$$

In the second case, in a similar way, we apply  $\psi_{p-1,q}^n, \psi_{p+1,q}^n, \psi_{p,q-1}^n, \psi_{p,q+1}^n, \psi_{p-1,q+1}^n, \psi_{p-1,q-1}^n, \psi_{p+1,q-1}^n, \psi_{p+1,q+1}^n \geq -1$  and find the condition for  $\psi_{pq}^{n+1} \geq -1$ ,

$$-1 \leq \psi_{pq}^n + \Delta t \left[ \frac{\psi_{pq}^n - (\psi_{pq}^n)^3}{\epsilon^2} - \frac{1}{3h^2} (10 + 10\psi_{pq}^n) \right] \leq \psi_{pq}^{n+1}. \quad (2.8)$$

Eq. (2.8) can be rewritten and simplified by dividing both sides by  $(1 + \psi_{pq}^n) > 0$

$$\begin{aligned}- (1 + \psi_{pq}^n) &\leq \Delta t (1 + \psi_{pq}^n) \left( \frac{\psi_{pq}^n (1 - \psi_{pq}^n)}{\epsilon^2} - \frac{10}{3h^2} \right), \\ -1 &\leq \Delta t \left( \frac{\psi_{pq}^n (1 - \psi_{pq}^n)}{\epsilon^2} - \frac{10}{3h^2} \right).\end{aligned}$$

Therefore, we can obtain the time step size  $\Delta t$  condition satisfying  $\psi_{pq}^{n+1} \geq -1$  as

$$\Delta t \leq \frac{3\epsilon^2 h^2}{10\epsilon^2 - 3h^2 \psi_{pq}^n (1 - \psi_{pq}^n)}.$$

Because  $\psi_{pq}^n (1 - \psi_{pq}^n) > 0$ , we obtain the condition satisfying  $|\psi_{pq}^{n+1}| \leq 1$  as  $\Delta t \leq 3h^2/10$ .

**Case 3.**  $-1 \leq \psi_{pq}^n < 0$ . Eq. (2.5) can be rewritten in the following by multiplying  $-1$  on both sides:

$$\begin{aligned}-\psi_{pq}^{n+1} &= -\psi_{pq}^n - \Delta t \left\{ \frac{-\psi_{pq}^n - (-\psi_{pq}^n)^3}{\epsilon^2} \right. \\ &\quad \left. + \frac{1}{6h^2} [4(-\psi_{p-1,q}^n - \psi_{p+1,q}^n - \psi_{p,q-1}^n - \psi_{p,q+1}^n) \right. \\ &\quad \left. - \psi_{p-1,q+1}^n - \psi_{p-1,q-1}^n - \psi_{p+1,q-1}^n - \psi_{p+1,q+1}^n + 20\psi_{pq}^n] \right\}.\end{aligned}$$

We define  $\psi_{pq}^n = -\psi_{pq}^n$ , then  $0 < \psi_{pq}^n \leq 1$ . Thus, we can obtain the following condition satisfying  $|\psi_{pq}^{n+1}| = |-\psi_{pq}^{n+1}| \leq 1$  by applying the proofs of Case 1 and Case 2:

$$\Delta t \leq \frac{3\epsilon^2 h^2}{6h^2 + 10\epsilon^2} < \frac{3h^2}{10}.$$

Here, the last inequality holds because the space step size  $h$  is nonzero positive number. Therefore, the following time step size  $\Delta t$  condition always satisfies  $|\psi_{pq}^{n+1}| \leq 1$ :

$$\Delta t \leq \frac{3\epsilon^2 h^2}{6h^2 + 10\epsilon^2}.$$

The proof is complete.  $\square$

The critical time step obtained from Theorem 2.1 is defined as

$$\Delta t_c = \frac{3\epsilon^2 h^2}{6h^2 \epsilon^2 + 10\epsilon^2}.$$

**Theorem 2.2.** Suppose that the initial condition satisfies

$$\max_{\substack{1 \leq p \leq N_x \\ 1 \leq q \leq N_y \\ 1 \leq r \leq N_z}} |\psi_{pqr}^0| \leq 1.$$

Then, the explicit isotropic scheme (2.2) ensures that the numerical solution remains bounded

$$|\psi_{pqr}^{n+1}| \leq 1, \quad p = 1, 2, \dots, N_x, \quad q = 1, 2, \dots, N_y, \quad r = 1, 2, \dots, N_z, \quad n \geq 0, \quad (2.9)$$

if the time step satisfies following conditions for 27-point and 19-point stencil discrete Laplacian operator, respectively

$$\Delta t \leq \frac{6h^2 \epsilon^2}{12h^2 + 25\epsilon^2}, \quad \Delta t \leq \frac{h^2 \epsilon^2}{2h^2 + 4\epsilon^2}.$$

*Proof.* The explicit isotropic method for the AC equation (2.2) is given as

$$\begin{aligned} \psi_{pqr}^{n+1} &= \psi_{pqr}^n + \Delta t \left[ \frac{\psi_{pqr}^n - (\psi_{pqr}^n)^3}{\epsilon^2} + \frac{1}{h^2(\alpha + 4\beta + 4\gamma)} \right. \\ &\quad \times \left( \alpha(\psi_{p+1,qr}^n + \psi_{p-1,qr}^n + \psi_{p,q+1,r}^n + \psi_{p,q-1,r}^n + \psi_{pq,r+1}^n + \psi_{pq,r-1}^n) \right. \\ &\quad + \beta(\psi_{p+1,q,r-1}^n + \psi_{p-1,q,r-1}^n + \psi_{p,q+1,r-1}^n + \psi_{p,q-1,r-1}^n + \psi_{p+1,q+1,r}^n \\ &\quad + \psi_{p-1,q+1,r}^n + \psi_{p+1,q-1,r}^n + \psi_{p-1,q-1,r}^n + \psi_{p+1,q,r+1}^n \\ &\quad + \psi_{p-1,q,r+1}^n + \psi_{p,q+1,r+1}^n + \psi_{p,q-1,r+1}^n) \\ &\quad + \gamma(\psi_{p+1,q+1,r-1}^n + \psi_{p-1,q+1,r-1}^n + \psi_{p+1,q-1,r-1}^n \\ &\quad + \psi_{p-1,q-1,r-1}^n + \psi_{p+1,q+1,r+1}^n + \psi_{p-1,q+1,r+1}^n \\ &\quad + \psi_{p+1,q-1,r+1}^n + \psi_{p-1,q-1,r+1}^n) \\ &\quad \left. \left. - (6\alpha + 12\beta + 8\gamma)\psi_{pqr}^n \right) \right]. \end{aligned} \quad (2.10)$$

**Case 1.**  $\psi_{pqr}^n = 1$ . Eq. (2.10) is given as

$$\psi_{pqr}^{n+1} = 1 + \frac{\Delta t}{h^2(\alpha + 4\beta + 4\gamma)} A_1, \quad (2.11)$$

where

$$\begin{aligned} A_1 &= \alpha(\psi_{p+1,qr}^n + \psi_{p-1,qr}^n + \psi_{p,q+1,r}^n + \psi_{p,q-1,r}^n + \psi_{pq,r+1}^n + \psi_{pq,r-1}^n) \\ &\quad + \beta(\psi_{p+1,q,r-1}^n + \psi_{p-1,q,r-1}^n + \psi_{p,q+1,r-1}^n + \psi_{p,q-1,r-1}^n + \psi_{p+1,q+1,r}^n + \psi_{p-1,q+1,r}^n \\ &\quad + \psi_{p+1,q-1,r}^n + \psi_{p-1,q-1,r}^n + \psi_{p+1,q,r+1}^n + \psi_{p-1,q,r+1}^n + \psi_{p,q+1,r+1}^n + \psi_{p,q-1,r+1}^n) \\ &\quad + \gamma(\psi_{p+1,q+1,r-1}^n + \psi_{p-1,q+1,r-1}^n + \psi_{p+1,q-1,r-1}^n + \psi_{p-1,q-1,r-1}^n + \psi_{p+1,q+1,r+1}^n \\ &\quad + \psi_{p-1,q+1,r+1}^n + \psi_{p+1,q-1,r+1}^n + \psi_{p-1,q-1,r+1}^n) - (6\alpha + 12\beta + 8\gamma). \end{aligned}$$

Because  $A_1 \leq 0$ , we have  $\psi_{pqr}^{n+1} \leq 1$ . If  $A_1 = 0$ , time step does not have a restriction. Else, when  $A_1 < 0$ , then  $\Delta t \leq 6h^2/25$  and  $\Delta t \leq h^2/4$  for 27-point ( $\alpha = 20/27, \beta = 2/9$ , and  $\gamma = 1/27$  [23]) and 19-point ( $\alpha = 2/3, \beta = 1/3$ , and  $\gamma = 0$ ) stencil discrete Laplacian operator, respectively results in  $\psi_{pqr}^{n+1} \geq -1$ . Therefore, we have  $|\psi_{pqr}^{n+1}| \leq 1$ . The 19-point stencil discrete Laplacian operator demonstrates higher efficiency compared to the 27-point stencil discrete Laplacian operator because the former uses fewer stencils than the latter in its computational process. However, it has stringent time-step constraints compared to the 27-point stencil discrete Laplacian operator.

**Case 2.**  $0 \leq \psi_{pqr}^n < 1$ . In Eq. (2.10), we consider the following two conditions of  $\Delta t$ : condition for  $\psi_{pqr}^{n+1} \leq 1$  and  $\psi_{pqr}^{n+1} \geq -1$ . For the first case, we apply  $\psi_{ijk}^n \leq 1$  for  $i = p-1, p, p+1$ ,  $j = q-1, q, q+1$ , and  $k = r-1, r, r+1$  to Eq. (2.10). Therefore the goal is to find  $\Delta t$  that satisfies the following inequality:

$$\begin{aligned} \psi_{pqr}^{n+1} \leq \psi_{pqr}^n + \Delta t \left\{ \frac{\psi_{pqr}^n - (\psi_{pqr}^n)^3}{\epsilon^2} + \frac{1}{h^2(\alpha + 4\beta + 4\gamma)} \right. \\ \left. \times [6\alpha + 12\beta + 8\gamma - (6\alpha + 12\beta + 8\gamma)\psi_{pqr}^n] \right\} \leq 1. \end{aligned} \quad (2.12)$$

Eq. (2.12) can be rewritten and simplified by dividing both sides by  $(1 - \psi_{pqr}^n) > 0$

$$\begin{aligned} \Delta t(1 - \psi_{pqr}^n) \left( \frac{\psi_{pqr}^n(1 + \psi_{pqr}^n)}{\epsilon^2} + \frac{6\alpha + 12\beta + 8\gamma}{h^2(\alpha + 4\beta + 4\gamma)} \right) \leq 1 - \psi_{pqr}^n, \\ \Delta t \left( \frac{\psi_{pqr}^n(1 + \psi_{pqr}^n)}{\epsilon^2} + \frac{6\alpha + 12\beta + 8\gamma}{h^2(\alpha + 4\beta + 4\gamma)} \right) \leq 1. \end{aligned}$$

Hence, we obtain the following  $\Delta t$  conditions satisfying  $\psi_{pqr}^{n+1} \leq 1$ :

$$\Delta t \leq \frac{(\alpha + 4\beta + 4\gamma)h^2\epsilon^2}{(\alpha + 4\beta + 4\gamma)h^2\psi_{pqr}^n(1 + \psi_{pqr}^n) + (6\alpha + 12\beta + 8\gamma)\epsilon^2}.$$

Because  $0 < \psi_{pqr}^n(1 + \psi_{pqr}^n) < 2$ , we obtain the generalized condition for 27-point stencil discrete Laplacian operator satisfying  $|\psi_{pqr}^{n+1}| \leq 1$  as follows:

$$\Delta t \leq \frac{(\alpha + 4\beta + 4\gamma)h^2\epsilon^2}{(\alpha + 4\beta + 4\gamma)2h^2 + (6\alpha + 12\beta + 8\gamma)\epsilon^2}.$$

If we take  $\alpha = 20/27, \beta = 2/9$ , and  $\gamma = 1/27$ , then we get

$$\Delta t \leq \frac{6h^2\epsilon^2}{12h^2 + 25\epsilon^2},$$

and if we take  $\alpha = 2/3, \beta = 1/3$ , and  $\gamma = 0$  for 19-point stencil discrete Laplacian operator we get

$$\Delta t \leq \frac{h^2\epsilon^2}{2h^2 + 4\epsilon^2}.$$

In the second case, we apply  $\psi_{ijk}^n \geq -1$  for  $i = p-1, p, p+1$ ,  $j = q-1, q, q+1$ , and  $k = r-1, r, r+1$  and find the condition of  $\Delta t$  for  $\psi_{pqr}^{n+1} \geq -1$ ,

$$\begin{aligned} \psi_{pqr}^{n+1} \geq \psi_{pqr}^n + \Delta t \left\{ \frac{\psi_{pqr}^n - (\psi_{pqr}^n)^3}{\epsilon^2} - \frac{1}{h^2(\alpha + 4\beta + 4\gamma)} \right. \\ \left. \times [6\alpha + 12\beta + 8\gamma + (6\alpha + 12\beta + 8\gamma)\psi_{pqr}^n] \right\} \geq -1. \end{aligned} \quad (2.13)$$

Eq. (2.13) can be rewritten and simplified by dividing both sides by  $(1 + \psi_{pqr}^n) > 0$

$$\begin{aligned} - (1 + \psi_{pq}^n) &\leq \Delta t (1 + \psi_{pqr}^n) \left( \frac{\psi_{pqr}^n (1 - \psi_{pqr}^n)}{\epsilon^2} - \frac{6\alpha + 12\beta + 8\gamma}{h^2(\alpha + 4\beta + 4\gamma)} \right), \\ - 1 &\leq \Delta t \left( \frac{\psi_{pqr}^n (1 - \psi_{pqr}^n)}{\epsilon^2} - \frac{6\alpha + 12\beta + 8\gamma}{h^2(\alpha + 4\beta + 4\gamma)} \right). \end{aligned}$$

Therefore, we can obtain the time step size  $\Delta t$  conditions satisfying  $\psi_{pqr}^{n+1} \geq -1$  as

$$\Delta t \leq \frac{(\alpha + 4\beta + 4\gamma)h^2\epsilon^2}{(6\alpha + 12\beta + 8\gamma)\epsilon^2 - (\alpha + 4\beta + 4\gamma)h^2\psi_{pqr}^n(1 - \psi_{pqr}^n)}.$$

Because  $\psi_{pqr}^n(1 - \psi_{pqr}^n) > 0$ , we obtain the generalized conditions for 27-point stencil discrete Laplacian operator satisfying  $|\psi_{pqr}^{n+1}| \leq 1$  as

$$\Delta t \leq \frac{(\alpha + 4\beta + 4\gamma)h^2}{6\alpha + 12\beta + 8\gamma}.$$

If we take  $\alpha = 20/27$ ,  $\beta = 2/9$ , and  $\gamma = 1/27$ , we get  $\Delta t \leq 6h^2/25$ , and if we take  $\alpha = 2/3$ ,  $\beta = 1/3$ , and  $\gamma = 0$  for 19-point stencil discrete Laplacian operator, we get  $\Delta t \leq h^2/4$ .

**Case 3.**  $-1 \leq \psi_{pq}^n < 0$ . Eq. (2.10) can be rewritten in the following by multiplying  $-1$  on both sides:

$$\begin{aligned} -\psi_{pqr}^{n+1} &= -\psi_{pqr}^n + \Delta t \left[ \frac{-\psi_{pqr}^n - (-\psi_{pqr}^n)^3}{\epsilon^2} + \frac{1}{h^2(\alpha + 4\beta + 4\gamma)} \right. \\ &\quad \times \left( \alpha(-\psi_{p+1,qr}^n - \psi_{p-1,qr}^n - \psi_{p,q+1,r}^n - \psi_{p,q-1,r}^n - \psi_{pq,r+1}^n - \psi_{pq,r-1}^n) \right. \\ &\quad + \beta(-\psi_{p+1,q,r-1}^n - \psi_{p-1,q,r-1}^n - \psi_{p,q+1,r-1}^n - \psi_{p,q-1,r-1}^n \\ &\quad - \psi_{p+1,q+1,r}^n - \psi_{p-1,q+1,r}^n - \psi_{p+1,q-1,r}^n - \psi_{p-1,q-1,r}^n \\ &\quad - \psi_{p+1,q,r+1}^n - \psi_{p-1,q,r+1}^n - \psi_{p,q+1,r+1}^n - \psi_{p,q-1,r+1}^n) \\ &\quad + \gamma(-\psi_{p+1,q+1,r-1}^n - \psi_{p-1,q+1,r-1}^n - \psi_{p+1,q-1,r-1}^n \\ &\quad - \psi_{p-1,q-1,r-1}^n - \psi_{p+1,q+1,r+1}^n - \psi_{p-1,q+1,r+1}^n \\ &\quad - \psi_{p+1,q-1,r+1}^n - \psi_{p-1,q-1,r+1}^n) \\ &\quad \left. \left. + (6\alpha + 12\beta + 8\gamma)(-\psi_{pqr}^n) \right) \right]. \end{aligned}$$

We define  $\zeta_{pq}^n = -\psi_{pqr}^n$ , then  $0 < \zeta_{pq}^n \leq 1$ . Thus, we can obtain the following conditions satisfying  $|\psi_{pqr}^{n+1}| = |-\psi_{pqr}^{n+1}| \leq 1$  by applying the proofs of Case 1 and Case 2. For 27-point stencil discrete Laplacian operator, we have

$$\Delta t \leq \frac{6h^2\epsilon^2}{12h^2 + 25\epsilon^2} < \frac{6h^2}{25}.$$

For 19-point stencil discrete Laplacian operator, we have

$$\Delta t \leq \frac{h^2\epsilon^2}{2h^2 + 4\epsilon^2} < \frac{h^2}{4}.$$

Here, the last two inequalities hold for 27-point and 19-point stencil discrete Laplacian operators, respectively, because the space step size  $h$  is a nonzero positive number. Therefore,

the following time step size  $\Delta t$  condition always satisfies  $|\psi_{pq}^{n+1}| \leq 1$  for 27-point and 19-point stencil discrete Laplacian operators:

$$\Delta t \leq \frac{6h^2\epsilon^2}{12h^2 + 25\epsilon^2}, \quad \Delta t \leq \frac{h^2\epsilon^2}{2h^2 + 4\epsilon^2}, \quad (2.14)$$

respectively.  $\square$

The maximum bound principle of the continuous AC equation [9] is preserved. If the initial and boundary values are limited to 1, then the solution remains within the same bound of 1. In [9], authors verified the existence in the limit of the AC equation interface evolving according to mean curvature motion. Consequently, the maximum principle is satisfied for both the continuous and discrete AC equations.

### 3. Computational Tests

To represent the thickness of the interfacial transition layer, a specific parameter is used as  $\epsilon_m = mh/[2\sqrt{2}\tanh^{-1}(0.9)]$ , which results in an interfacial transition layer thickness of approximately  $mh$ , where  $m$  is a positive integer, as described in [13]. In the subsequent simulations, we adopt  $\epsilon = \epsilon_m$  for suitable values of  $m$ .

#### 3.1. Comparison test

We compare the computational solutions obtained by using the standard and isotropic discrete Laplacian operators. In two-dimensional space, the standard discrete Laplacian operator is defined on the 2D domain  $\Omega = (-1, 1) \times (-1, 1)$  as follows:

$$\Delta_s \psi_{pq} = \frac{1}{h^2} (\psi_{p-1,q} + \psi_{p+1,q} - 4\psi_{pq} + \psi_{p,q-1} + \psi_{p,q+1}).$$

Let us consider the initial condition as

$$\psi(x, y, 0) = 0.5 \left[ 1 + \frac{\tanh(0.1 - \sqrt{x^2 + y^2})}{\sqrt{2}\epsilon} \right].$$

We consider the solution to the AC equation with the standard and isotropic discrete Laplacian operators. Here, we use  $N_x = N_y = 80$ ,  $h = 1/40$ ,  $\epsilon = h/2$ , and  $\Delta t = (\epsilon^2 h^2)/(6h^2 + 10\epsilon^2)$ . Fig. 3.1 shows the zero-level contour of the computational solutions at  $t = 100\Delta t$  for the standard and isotropic discrete Laplacian operators with a reference circle. As shown in Fig. 3.1, the zero-level contour obtained using the isotropic discrete Laplacian operator follows the reference circle, in contrast to the standard discrete Laplacian operator that shows an anisotropic shape.

Next, we consider the quantitative comparison between standard and isotropic Laplacian operators. The discrete  $l_2$ -error is defined as

$$\|\psi^{N_t}\|_2 = \sqrt{\sum_{q=1}^{N_y} \sum_{p=1}^{N_x} \frac{(\psi_{pq}^{N_t})^2}{N_x N_y}},$$

and discrete maximum norm is defined as

$$\|\psi^{N_t}\|_{\max} = \max_{1 \leq p \leq N_x, 1 \leq q \leq N_y} |\psi_{pq}^{N_t}|.$$

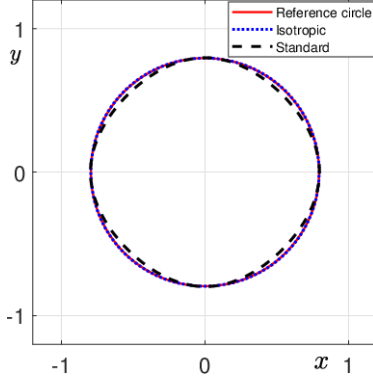


Fig. 3.1. Zero-level contour of the computational solutions for the standard and isotropic discrete Laplacian operators with a reference circle. Here, time  $t = 100\Delta t$ .

Then, we define the  $l_2$ -error and max-error between  $\psi^{N_t}$  and  $\bar{\psi}^{N_t}$  as

$$\sqrt{\sum_{q=1}^{N_y} \sum_{p=1}^{N_x} \frac{(\psi_{pq}^{N_t} - \bar{\psi}_{pq}^{N_t})^2}{N_x N_y}} \quad \text{and} \quad \max_{1 \leq p \leq N_x, 1 \leq q \leq N_y} |\psi_{pq}^{N_t} - \bar{\psi}_{pq}^{N_t}|,$$

respectively. We consider the following initial condition on  $\Omega = (-1, 1) \times (-1, 1)$ :

$$\psi(x, y, 0) = 0.5 \left( 1 + \tanh \left( \frac{0.3 - \sqrt{x^2 + y^2}}{2\sqrt{2}\epsilon} \right) \right).$$

The parameters used are  $\Delta t = 2.5e-7$ , final time  $T = 4200\Delta t$ , and  $\epsilon = h$ . The transition layer thickness of the computational solution of the AC equation is constantly adjusted by  $\epsilon$ . Therefore, to compare standard and isotropic Laplacian operators, we define the function  $g(r, x, y)$  on  $\Omega$  with a thickness of the transition layer equal to the transition layer thickness of the initial condition as follows:

$$g(r, x, y) = 0.5 \left( 1 + \tanh \left( \frac{r - \sqrt{x^2 + y^2}}{2\sqrt{2}\epsilon} \right) \right).$$

We find the optimal value of the parameter  $r$  that best fits the numerical solutions at the final time  $T$  in the least-squares sense

$$\min_r \sum_{i=1}^{N_x} \sum_{j=1}^{N_y} (\psi_{ij}^{N_t} - g(r, x_i, y_j))^2.$$

To obtain the optimal  $r$  for the function  $g(r, x, y)$  that fits the numerical solution  $\psi_{ij}^{N_t}$ , we use the nonlinear curve-fitting function `lsqcurvefit` in MATLAB R2022b, which is a nonlinear least-squares optimization function [33]

$$R = \text{lsqcurvefit}('g', r_0, \Omega^h, \psi^{N_t}),$$

where  $r_0$  is initial radius and  $\psi^{N_t} = \{\psi_{ij}^{N_t} \mid i = 1, 2, \dots, N_x, j = 1, 2, \dots, N_y\}$  on  $\Omega^h$ . The calculated optimized values for the numerical solutions of AC equation using the standard and isotropic Laplacian operators are represented by  $R_1$  and  $R_2$ , respectively. Fig. 3.2 shows

the differences between  $g(R, x, y)$  with optimized  $R$  and the numerical solutions using the standard and isotropic Laplacian operators at the final time  $T$ . Fig. 3.3 shows the  $g(R, x, y)$  with optimized  $R$  and numerical solutions at the final time  $T$ , according to the distance  $\sqrt{x^2 + y^2}$  from the center  $(0, 0)$  to  $(x, y)$ . Table 3.1 lists the  $l_2$ -error and max-error between  $g(R, x, y)$  with optimized  $R$  and the numerical solutions using the standard and isotropic Laplacian operators at the final time  $T$ . We observe that numerical solutions using the standard Laplacian operator

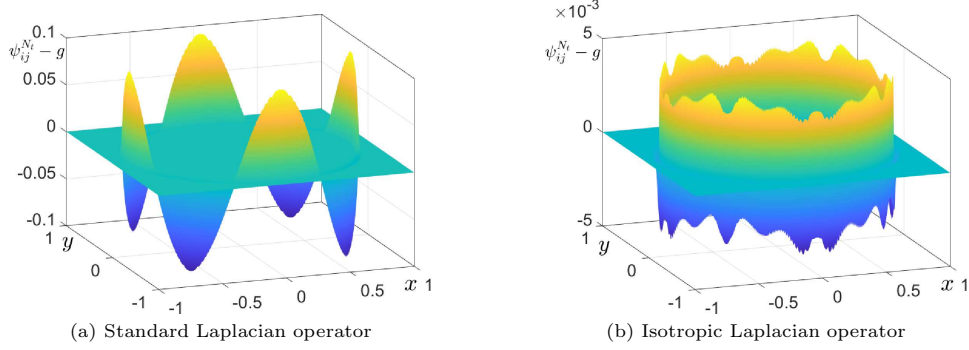


Fig. 3.2. The differences between  $g(R, x, y)$  with optimized  $R$  and the numerical solutions using the standard and isotropic Laplacian operators at the final time  $T$ .

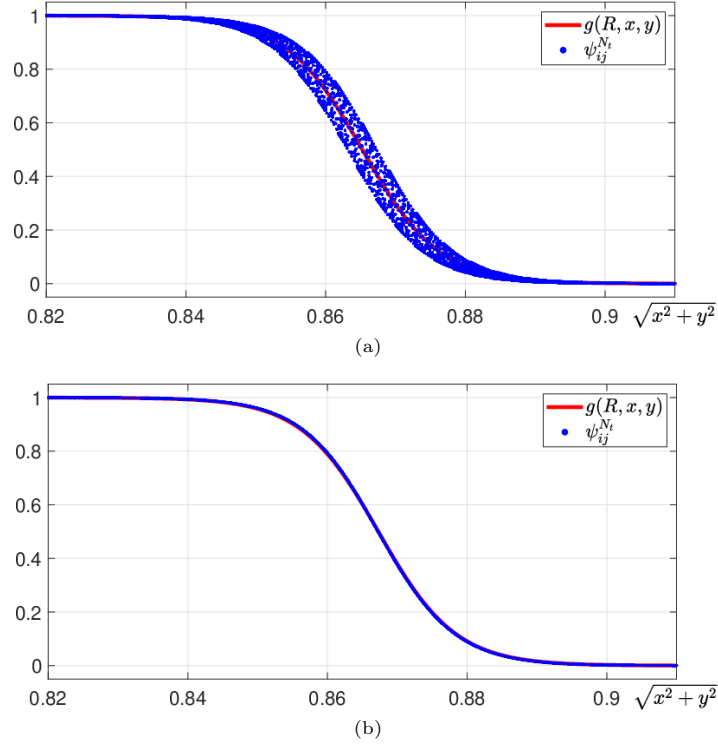


Fig. 3.3. (a) Numerical solution using the standard Laplacian operator and  $g(R, x, y)$  with optimized value  $R$ , (b) Numerical solution using the isotropic Laplacian operator and  $g(R, x, y)$  with optimized value  $R$ .

Table 3.1:  $l_2$ -error and max-error between  $g(R, x, y)$  with optimized  $R$  and the numerical solutions using the standard and isotropic Laplacian operators at the final time  $T$ .

	Standard Laplacian	Isotropic Laplacian
$l_2$ -error	9.6594e-3	5.7557e-4
max-error	9.8167e-2	4.4827e-3

are not consistent at the points with the same distance  $\sqrt{x^2 + y^2}$ . On the other hand, we observe that numerical solutions using the isotropic Laplacian operator satisfy isotropy, and obtain consistent numerical solutions at the points with the same distance  $\sqrt{x^2 + y^2}$ .

### 3.2. Maximum principle for time steps

We consider a numerical experiment which confirms the time step restriction required for the maximum principle and it is a sharp estimation. The initial condition is given as

$$\psi(x, y, 0) = \begin{cases} \psi, & \text{if } x = 0, \quad y = 0, \\ 1, & \text{otherwise,} \end{cases}$$

where  $\psi$  is a number between 0 and 1. We use  $\Delta t = 1.01\Delta t_p$ , where

$$\Delta t_p = \frac{3\epsilon^2 h^2}{3h^2\psi(1 + \psi) + 10\epsilon^2}$$

is the maximum time step derived in Case 2 of Theorem 2.1. Fig. 3.4 shows the ratio of  $\Delta t/\Delta t_c$  and the value of  $\psi(0, 0, \Delta t)$  according to the variation of  $\psi$ . Furthermore, we considered stable time step  $\Delta t = 0.99\Delta t_p$ . Fig. 3.4(a) also shows results with  $\Delta t = 0.99\Delta t_p$ . In Fig. 3.4(b), spatial step size  $\Delta t = 0.99\Delta t_p$  is stable and preserves the maximum principle.

In 3D space, the following initial condition is applied on the domain  $(-1, 1) \times (-1, 1) \times (-1, 1)$ :

$$\psi(x, y, z, 0) = \begin{cases} \psi, & x = 0, \quad y = 0, \quad z = 0, \\ 1, & \text{otherwise,} \end{cases}$$

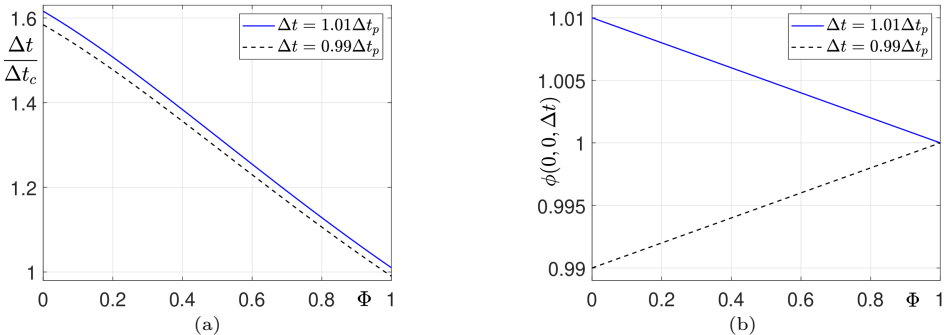


Fig. 3.4. (a) is the ratio of  $\Delta t$  to  $\Delta t_c$  that depends on value of  $\psi$ . (b) is the value of  $\psi(0, 0, \Delta t)$  that depends on value of  $\psi$ .

For simplicity of the test, we take  $N_x = N_y = N_z = 11$ ,  $h = 2/11$ , and  $\epsilon = h$ . We define the following time restrictions derived in Theorem 2.2:

$$\Delta t_p = \frac{(\alpha + 4\beta + 4\gamma)h^2}{\psi(1 + \psi)(\alpha + 4\beta + 4\gamma) + 6\alpha + 12\beta + 8\gamma},$$

$$\Delta t_c = \frac{(\alpha + 4\beta + 4\gamma)h^2}{2(\alpha + 4\beta + 4\gamma) + 6\alpha + 12\beta + 8\gamma},$$

which are dependent and independent on  $\psi$ , respectively. The ratio of above two time step restrictions can be written as

$$\frac{\Delta t_p}{\Delta t_c} = \frac{2(\alpha + 4\beta + 4\gamma) + 6\alpha + 12\beta + 8\gamma}{\psi(1 + \psi)(\alpha + 4\beta + 4\gamma) + 6\alpha + 12\beta + 8\gamma}.$$

In Fig. 3.5, we consider two time steps  $\Delta t = 1.01\Delta t_p$  and  $\Delta t = 0.99\Delta t_p$  for  $0 \leq \psi \leq 1$ . Figs. 3.5(a)-(b) and 3.5(c)-(d) show the results of 27- and 19-point stencil discrete isotropic Laplacian operator, respectively. Figs. 3.5(a) and 3.5(c) show the ratio of  $\Delta t_p$  and  $\Delta t_c$ . Figs. 3.5(b) and 3.5(d) represent the values of  $\psi(0, 0, 0, \Delta t)$  with respect to  $0 \leq \psi \leq 1$  for  $\Delta t = 1.01\Delta t_p$  and  $\Delta t = 0.99\Delta t_p$ . From the results of Fig. 3.5, the maximum principle is not preserved when the time step does not satisfy analytical restriction.

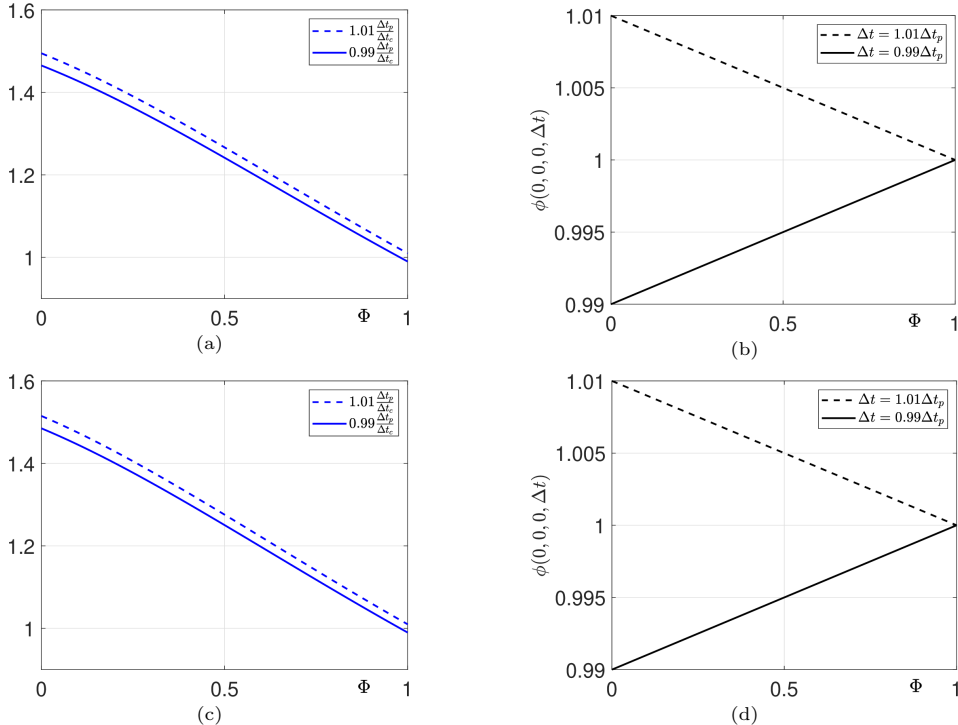


Fig. 3.5. (a) Ratio of  $\Delta t_p$  and  $\Delta t_c$  and (b)  $\psi(0, 0, 0, \Delta t)$  respect to  $\psi$  for 27-point discrete isotropic Laplacian operator. (c) Ratio of  $\Delta t_p$  and  $\Delta t_c$  and (d)  $\psi(0, 0, 0, \Delta t)$  respect to  $\psi$  for 19-point discrete isotropic Laplacian operator.

### 3.3. Convergence test for time step in 2D

For convergence test, we employ a traveling wave solution [41]

$$\psi_{exact}(x, y, t) = \frac{1}{2} \left[ 1 - \tanh \left( \frac{x - 0.15 - 3t/(\sqrt{2}\epsilon)}{2\sqrt{2}\epsilon} \right) \right]. \quad (3.1)$$

To assess the convergence of the 2D AC equation, we utilized the spatial step size stability condition, which was found by the analysis of Theorem 2.1 and defined in Eq. (2.4) as  $\Delta t = (3\epsilon^2 h^2)/(6h^2 + 10\epsilon^2)$ . In Fig. 3.6, we use the following time steps:  $\Delta t$ ,  $0.5\Delta t$ ,  $0.25\Delta t$ , and  $0.125\Delta t$  on computational domain  $\Omega = (0, 1) \times (0, 1)$  with  $N = 200$ ,  $h = 0.005$ ,  $\epsilon = \epsilon_{10}$ , and  $T = 300\Delta t$ . The discrete error for the proposed method is defined as  $\mathbf{e}^{N_t} = (e_1^{N_t}, e_2^{N_t}, \dots, e_N^{N_t})$ , where

$$e_{pq}^{N_t} = \psi_{(x_p, y_q)}^{N_t} - \psi_{exact}(x_p, y_q, N_t\Delta t).$$

Corresponding discrete  $l_2$ -error is defined as

$$\|\mathbf{e}^{N_t}\|_2 = \sqrt{\sum_{q=1}^{N_y} \sum_{p=1}^{N_x} \frac{(e_{pq}^{N_t})^2}{N_x N_y}},$$

and max-error as

$$\|\mathbf{e}^{N_t}\|_{\max} = \max_{1 \leq p \leq N_x, 1 \leq q \leq N_y} |e_{pq}^{N_t}|.$$

Let  $\log_2(\|\mathbf{e}^{N_t}\|/\|\mathbf{e}^{2N_t}\|)$  be a time convergence rate. Table 3.2 provides information about errors and temporal convergence rates associated with both  $l_2$ - and max-error measurements.

However, if we choose time step slightly larger, i.e.  $1.01 \times \Delta t$  which is larger than the stable time step  $\Delta t = (3\epsilon^2 h^2)/(6h^2 + 10\epsilon^2)$  we found, both  $L_2$  and maximum norm convergence rate of

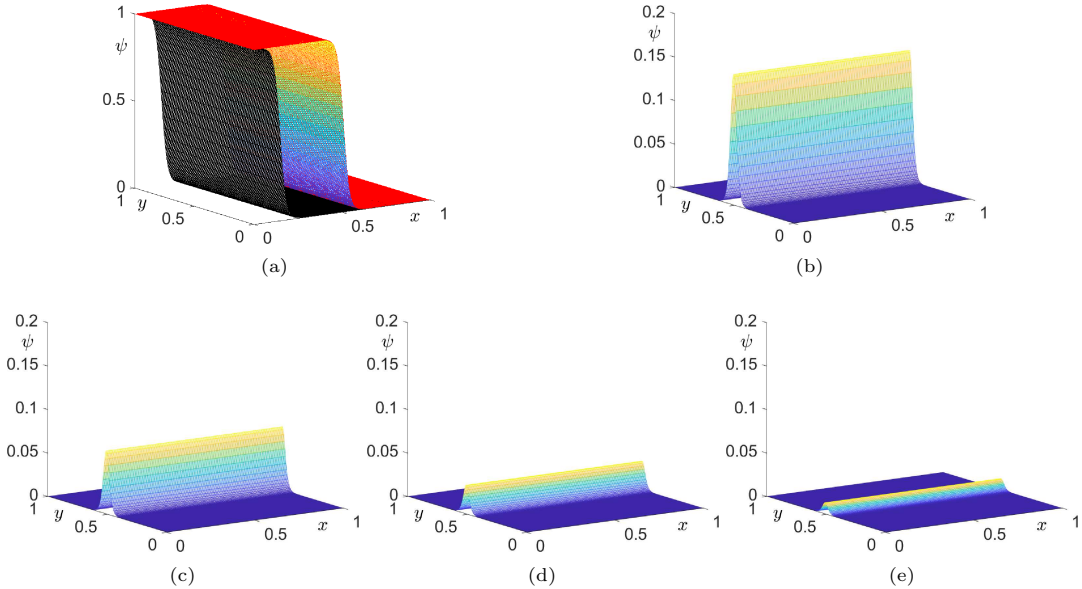


Fig. 3.6. (a) contain initial condition (black) of 2D AC equation with numerical result (RGB) and exact solution (red) at  $t = 0.002$ . (b)-(e) are decrement in errors when  $\Delta t = (3\epsilon^2 h^2)/(6h^2 + 10\epsilon^2)$ ,  $0.5\Delta t$ ,  $0.25\Delta t$ , and  $0.125\Delta t$ , respectively.

the scheme become unstable  $-1.04275$ ,  $-1.01377$ , respectively. However, Table 3.2 verifies that the system remains stable when using the examined time intervals and demonstrates first-order temporal accuracy.

Furthermore, we investigate the accuracy of proposed algorithm using the 3D AC equation. We use the traveling wave solution

$$\psi_{exact}(x, y, z, t) = \frac{1}{2} \left[ 1 - \tanh \left( \frac{x - 0.15 - 3t/(\sqrt{2}\epsilon)}{2\sqrt{2}\epsilon} \right) \right].$$

We set the initial condition  $\psi(x, y, z, 0) = \psi_{exact}(x, y, z, 0)$  on  $\Omega = (0, 1) \times (0, 0.1) \times (0, 0.1)$ . Here, the parameters used are  $h = 0.005$ ,  $\epsilon = \epsilon_{10}$ , and  $T = 150\Delta t$ . Tables 3.3 and 3.4 show the errors and convergence rates with 19- and 27-point stencils, respectively. In addition, the difference between the  $l_2$ -error and max-error can be understood from Fig. 3.6(b)-(e) that illustrate the errors. The error is large on the middle part of the computational domain, while it is negligible elsewhere. The same phenomenon is observed at 3D computations. Therefore, the  $l_2$ -error and max-error shows significant difference in Tables 3.3 and 3.4.

Table 3.2: Temporal errors and convergence rates at  $t = T$  for 2D AC equation.

$\Delta t$	$\Delta t = (3\epsilon^2 h^2)/(6h^2 + 10\epsilon^2)$		$0.5\Delta t$		$0.25\Delta t$		$0.125\Delta t$
$l_2$ -error	0.0316202		0.0153158		0.00692684		0.00267657
Rate		1.04583		1.14475		1.37181	
max-error	0.150264		0.072707		0.0330002		0.0129383
Rate		1.04733		1.13962		1.35082	

Table 3.3: Temporal errors and convergence rates with 19-point stencil.

$\Delta t$	$\Delta t = (3\epsilon^2 h^2)/(6h^2 + 10\epsilon^2)$		$0.5\Delta t$		$0.25\Delta t$		$0.125\Delta t$
$l_2$ -error	9.73894e-04		4.79849e-04		2.28086e-04		1.01165e-04
Rate		1.02		1.07		1.17	
max-error	4.70945e-02		2.33185e-02		1.12012e-02		5.09120e-03
Rate		1.01		1.06		1.14	

Table 3.4: Temporal errors and convergence rates with 27-point stencil.

$\Delta t$	$\Delta t = (3\epsilon^2 h^2)/(6h^2 + 10\epsilon^2)$		$0.5\Delta t$		$0.25\Delta t$		$0.125\Delta t$
$l_2$ -error	8.95058e-04		4.41056e-04		2.09906e-04		9.34524e-05
Rate		1.02		1.07		1.17	
max-error	4.32952e-02		2.14458e-02		1.03214e-02		4.71203e-03
Rate		1.01		1.06		1.13	

### 3.4. Motion by mean curvature

The focus of this section is on examining the numerical solution specified on the mean curvature flow. It is well known that the zero-level interface of the AC equation solution

conforms to motion by mean curvature as  $\epsilon$  approaches zero. Therefore, we choose the time step restrictions  $\Delta t$  for 27-point and 19-point stencil discrete Laplacian operator that are obtained through explicit isotropic finite difference scheme defined in Eq. (2.14). Our objective is to illustrate the scheme's stability when utilizing the applied time steps. To achieve this, we observe progressing numerical solutions and validate inherent properties of the AC equation, such as the mean curvature flow behavior. In the forthcoming tests, we adopt a specific value for the interface parameter thickness, denoted as  $\epsilon = \epsilon_{10}$ .

We consider a 3D computational domain  $\Omega = (-1, 1) \times (-1, 1) \times (-1, 1)$ . We use  $96 \times 96 \times 96$  mesh with mesh size  $h = 2/96$ , and spatial step size  $\Delta t = \epsilon^2 h^2 / (2h^2 + 4\epsilon^2)$  and  $\Delta t = 6\epsilon^2 h^2 / (12h^2 + 25\epsilon^2)$  for 19-point and 27-point stencil discrete Laplacian operator respectively. The initial condition is given as

$$\psi(x, y, z, 0) = \tanh\left(\frac{R_0 - \sqrt{x^2 + y^2 + z^2}}{\sqrt{2}\epsilon}\right) \quad (3.2)$$

with  $R_0 = 0.7$ . The theoretical radius of the 3D sphere is given as  $R(t) = \sqrt{R_0 - 4t}$ .

Figs. 3.7 and 3.8(a)-(c) depict the temporal evolution of the zero-level isosurface of the AC equation solution, while Figs. 3.7 and 3.8(d) present the variation in analytic and numerical radii over time  $t$  for 27-point and 19-point stencil discrete Laplacian operator respectively. The findings from Figs. 3.7 and 3.8 collectively demonstrate that, for the explicit scheme, the examined time step ensures scheme stability, and the solutions faithfully adhere to the motion by mean curvature.

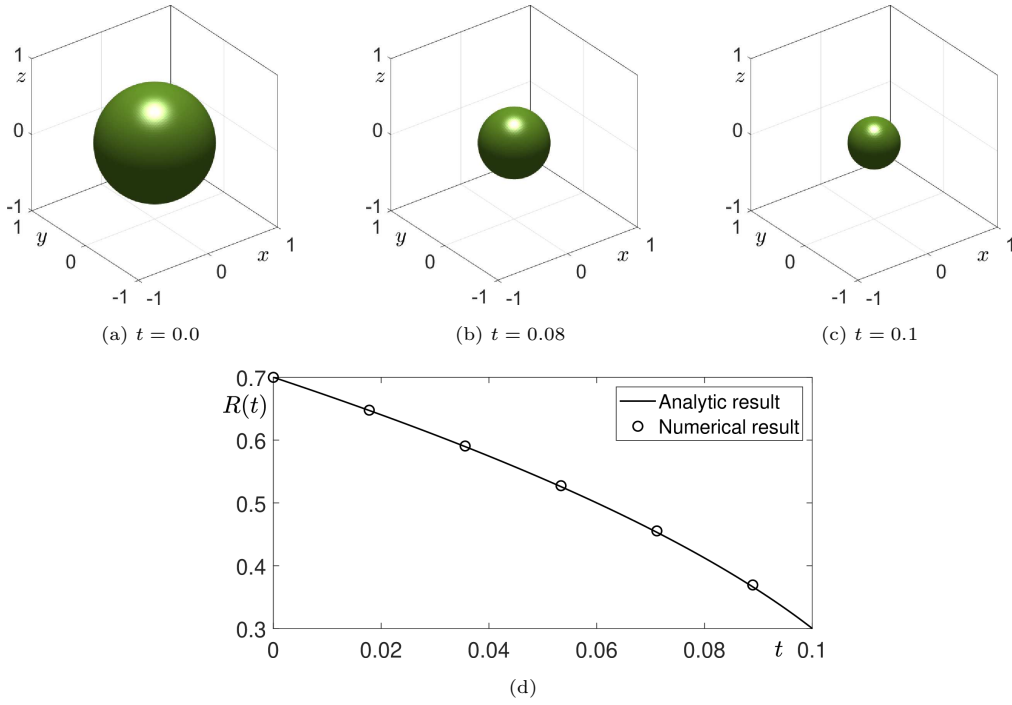


Fig. 3.7. (a)-(c) Temporal progression of the numerical solutions illustrated as an isosurface when  $\Delta t = (6\epsilon^2 h^2) / (12h^2 + 25\epsilon^2)$ . (d) Comparison of the analytical and numerical radius changes as a function of time using 27-point stencil discrete Laplacian operator.

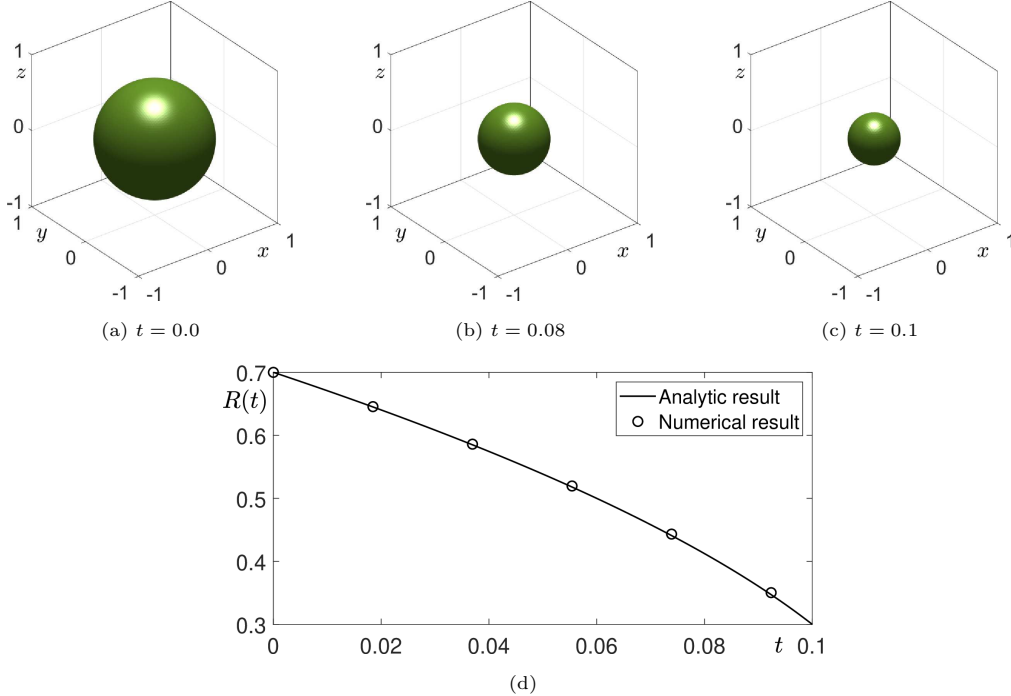


Fig. 3.8. (a)-(c) Temporal progression of the numerical solutions illustrated as an isosurface when  $\Delta t = (\epsilon^2 h^2)/(2h^2 + 4\epsilon^2)$ . (d) Comparison of the analytical and numerical radius changes as a function of time using 19-point stencil discrete Laplacian operator.

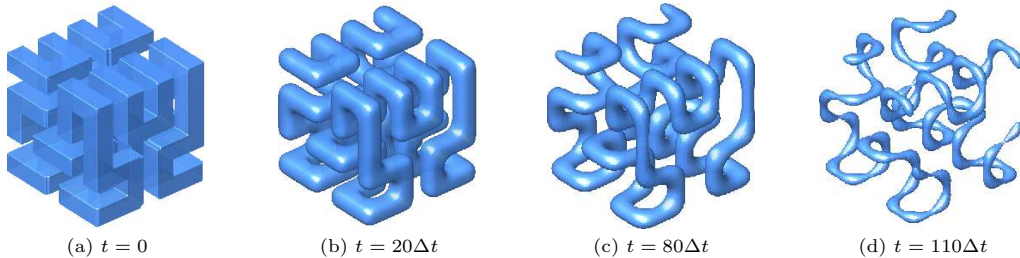


Fig. 3.9. Temporal progression of the numerical solutions illustrated as an isosurface with 19-point stencil discrete Laplacian operator.

Now, we study the mean curvature flow for a complex geometry in the three-dimensional domain  $(-1, 1) \times (-1, 1) \times (-1, 1)$ . We consider a complex initial condition illustrated in Fig. 3.9(a). Figs. 3.9(a)-(d) illustrate the temporal progression of zero-level isosurfaces of the numerical solutions at the zero-level to the AC equation with 19-point stencil discrete Laplacian operator. Here,  $\Delta t = \epsilon^2 h^2/(2h^2 + 4\epsilon^2)$  is used and the time  $t$  is shown below each figure.

#### 4. Conclusions

A fully explicit FDM for the AC equation is fast and accurate, however, conventional finite difference scheme: the emergence of anisotropy due to directional bias in error terms, which markedly influences interface dynamics. To resolve this issue, we introduced an isotropic FDM

to solve the AC equation. In the context of isotropic stencils, there exists only a single option for the 2D configuration at the lowest order, i.e. 9-point isotropic stencil, whereas there are numerous options for 3D configuration. Among various options, we used 19- and 27-point isotropic stencil to solve AC equation in 3D. We studied the maximum principle of the explicit isotropic method and determined optimal time step limitations in both 2D and 3D domains. Computational tests verified the maximum principle under the theoretical time step restriction. In 2D space, the convergence test is performed using the traveling wave solution. Both  $l_2$ -error and max-error are used for calculating the convergence rate. Furthermore, we studied the mean curvature flow of the computational solutions in 3D space, showing good agreement between the theoretical and numerical solution. For future work, we can apply isotropic FDM to solve other phase field equations like the Cahn-Hilliard equation [22,45]. In addition, we will investigate the maximum principle of isotropic finite difference schemes based on the Crank-Nicolson, second-order backward differentiation formula, and implicit-explicit schemes, as referred in [8,14,15,39]. When applying the Crank-Nicolson scheme, variable time step [3, 17, 34] can be applied for improvement in stability and computational efficiency.

**Acknowledgments.** The authors extend their thanks to the reviewers for the valuable and constructive input they provided during the revision of the article.

The first author (Jyoti) was supported by the Brain Pool program funded by the Ministry of Science and ICT through the National Research Foundation of Korea (Grant No. 2022H1D3A2A02081237). The corresponding author (J.S. Kim) was supported by the National Research Foundation of Korea grant funded by the Korea government (MSIT) (Grant No. 2022R1A2C1003844).

## References

- [1] S.M. Allen and J.W. Cahn, A microscopic theory for antiphase boundary motion and its application to antiphase domain coarsening, *Acta Metall.*, **27**:6 (1979), 1085–1095.
- [2] M.B. Amar and E. Brener, Theory of pattern selection in three-dimensional nonaxisymmetric dendritic growth, *Phys. Rev. Lett.*, **71**:4 (1993), 589.
- [3] T. Apel and T.G. Flaig, Crank-Nicolson schemes for optimal control problems with evolution equations, *SIAM J. Numer. Anal.*, **50**:3 (2012), 1484–1512.
- [4] H. Assadi, A phase-field model for non-equilibrium solidification of intermetallics, *Acta Metall.*, **55**:15 (2007), 5225–5235.
- [5] N. Batangouna, A robust family of exponential attractors for a time semi-discretization of the Ginzburg-Landau equation, *AIMS Math.*, **7**:1 (2022), 1399–1415.
- [6] R. Chen, X. Yang, and H. Zhang, Decoupled, energy stable scheme for hydrodynamic Allen-Cahn phase field moving contact line model, *J. Comp. Math.*, **36**:5 (2018), 661–681.
- [7] Q. Chu, G. Jin, J. Shen, and Y. Jin, Numerical analysis of Crank-Nicolson scheme for the Allen-Cahn equation, *J. Comp. Math.*, **39**:5 (2021), 655.
- [8] Y. Deng and Z. Weng, Barycentric interpolation collocation method based on Crank-Nicolson scheme for the Allen-Cahn equation, *AIMS Math.*, **6**:4 (2021), 3857–3873.
- [9] L.C. Evans, H.M. Soner, and P.E. Souganidis, Phase transitions and generalized motion by mean curvature, *Commun. Pure Appl. Math.*, **45**:9 (1992), 1097–1123.
- [10] Z. Gao, H. Zhang, X. Qian, and S. Song, High-order unconditionally maximum-principle-preserving parametric integrating factor Runge-Kutta schemes for the nonlocal Allen-Cahn equation, *Appl. Numer. Math.*, **194** (2023), 97–114.
- [11] Y. Gong, B. Ji, and H.L. Liao, A maximum bound principle preserving iteration technique for a class of semilinear parabolic equations, *Appl. Numer. Math.*, **184** (2023), 482–495.

- [12] X. Gu, Y. Wang, and W. Cai, Energy stable and maximum bound principle preserving schemes for the Allen-Cahn equation based on the Saul'yev methods, *Adv. Comput. Math.*, **50**:3 (2024), 34.
- [13] S. Ham and J. Kim, Stability analysis for a maximum principle preserving explicit scheme of the Allen-Cahn equation, *Math. Comput. Simul.*, **207** (2023), 453–465.
- [14] D. Hou, L. Ju, and Z. Qiao, A linear second-order maximum bound principle-preserving BDF scheme for the Allen-Cahn equation with a general mobility, *Math. Comput.*, **92**:344 (2023) 2515–2542.
- [15] T. Hou, T. Tang, and J. Yang, Numerical analysis of fully discretized Crank-Nicolson scheme for fractional-in-space Allen-Cahn equations, *J. Sci. Comput.*, **72** (2017), 1214–1231.
- [16] D. Jeong, Y. Li, Y. Choi, C. Lee, J. Yang, and J. Kim, A practical adaptive grid method for the Allen-Cahn equation, *Physica A*, **573** (2021), 125975.
- [17] B. Ji, H.L. Liao, Y. Gong, and L. Zhang, Adaptive second-order Crank-Nicolson time-stepping schemes for time-fractional molecular beam epitaxial growth models, *SIAM J. Sci. Comput.*, **42**:3 (2020), B738–B760.
- [18] K. Ji, A.M. Tabrizi, and A. Karma, Isotropic finite-difference approximations for phase-field simulations of polycrystalline alloy solidification, *J. Comput. Phys.*, **457** (2022), 111069.
- [19] B. Jiang, Q. Xia, J. Kim, and Y. Li, Efficient second-order accurate scheme for fluid–surfactant systems on curved surfaces with unconditional energy stability, *Commun. Nonlinear Sci. Numer. Simul.*, **135** (2024), 108054.
- [20] Z.F. Khankishiyev, Solution of one problem for a loaded differential equation by the method of finite differences, *Appl. Numer. Math.*, **21**:2 (2022), 147–157.
- [21] H. Kim, S. Yoon, J. Wang, C. Lee, S. Kim, J. Park, and J. Kim, Shape transformation using the modified Allen-Cahn equation, *Appl. Math. Lett.*, **107** (2020), 106487.
- [22] J. Kim, Z. Tan, and J. Yang, Linear and conservative IMEX Runge-Kutta finite difference schemes with provable energy stability for the Cahn-Hilliard model in arbitrary domains, *Comput. Math. Appl.*, **143** (2023), 133–150.
- [23] A. Kumar, Isotropic finite-differences, *J. Comput. Phys.*, **201**:1 (2004), 109–118.
- [24] S. Lai, Q. Xia, J. Kim, and Y. Li, Phase-field based modeling and simulation for selective laser melting techniques in additive manufacturing, *Commun. Nonlinear Sci. Numer. Simul.*, **138** (2024), 108239.
- [25] J.S. Langer, Dendrites, viscous fingers, and the theory of pattern formation, *Science*, **243**:4895 (1989), 1150–1156.
- [26] D. Lee, Computing the area-minimizing surface by the Allen-Cahn equation with the fixed boundary, *AIMS Math.*, **8**:10 (2023), 23352–23371.
- [27] D. Lee and S. Lee, Image segmentation based on modified fractional Allen-Cahn equation, *Math. Probl. Eng.*, **2019**:1 (2019), 3980181.
- [28] H.G. Lee, S. Ham, and J. Kim, Isotropic finite difference discretization of Laplacian operator, *Appl. Comput. Math.*, **22**:2 (2023), 259–274.
- [29] J. Li, J. Zeng, and R. Li, An adaptive discontinuous finite volume element method for the Allen-Cahn equation, *Adv. Comput. Math.*, **49**:4 (2023), 55.
- [30] R. Li, Y. Gao, and Z. Chen, Adaptive discontinuous Galerkin finite element methods for the Allen-Cahn equation on polygonal meshes, *Numer. Algorithms*, **95**:4 (2024), 1981–2014.
- [31] Y. Li, Q. Xia, C. Lee, S. Kim, and J. Kim, A robust and efficient fingerprint image restoration method based on a phase-field model, *Pattern Recognit.*, **123** (2022), 108405.
- [32] X. Liu, Q. Hong, H.L. Liao, and Y. Gong, A multi-physical structure-preserving method and its analysis for the conservative Allen-Cahn equation with nonlocal constraint, *Numer. Algorithms*, **97**:3 (2024), 1431–1451.
- [33] C.P. López, Optimization techniques via the optimization toolbox, in: *MATLAB Optimization Techniques*, Apress, (2014), 85–108.
- [34] A.A. Medovikov and V.I. Lebedev, Variable time steps optimization of L  $\omega$ -stable Crank-Nicolson

- method, *Russ. J. Numer. Anal. Math. Model.*, **20**:3 (2005), 283–303.
- [35] X. Qi, Y. Zhang, and C. Xu, An efficient approximation to the stochastic Allen-Cahn equation with random diffusion coefficient field and multiplicative noise, *Adv. Comput. Math.*, **49**:5 (2023), 73.
  - [36] Z. Şen and A. Khanmamedov, The Cahn-Hilliard/Allen-Cahn equation with inertial and proliferation terms, *J. Math. Anal. Appl.*, **530**:2 (2024), 127736.
  - [37] J. Shen, T. Tang, and J. Yang, On the maximum principle preserving schemes for the generalized Allen-Cahn equation, *Commun. Math. Sci.*, **14**:6 (2016), 1517–1534.
  - [38] T. Suzuki, K. Takasao, and N. Yamazaki, New approximate method for the Allen-Cahn equation with double-obstacle constraint and stability criteria for numerical simulations, *AIMS Math.*, **1**:3 (2016), 288–317.
  - [39] T. Tang and J. Yang, Implicit-explicit scheme for the Allen-Cahn equation preserves the maximum principle, *J. Comp. Math.*, (2016), 451–461.
  - [40] J. Wang, Z. Han, and J. Kim, An efficient and explicit local image inpainting method using the Allen-Cahn equation, *Z. Angew. Math. Phys.*, **75**:2 (2024), 44.
  - [41] A.M. Wazwaz, The Tanh-Coth method for solitons and kink solutions for nonlinear parabolic equations, *Appl. Math. Comput.*, **188**:2 (2007), 1467–1475.
  - [42] Q. Xia, J. Yang, J. Kim, and Y. Li, On the phase field based model for the crystalline transition and nucleation within the Lagrange multiplier framework, *J. Comput. Phys.*, **513** (2024), 113158.
  - [43] Q. Xia, X. Jiang, and Y. Li, A modified and efficient phase field model for the biological transport network, *J. Comput. Phys.*, **488** (2023), 112192.
  - [44] Q. Xia, J. Zhu, Q. Yu, J. Kim, and Y. Li, Triply periodic minimal surfaces based topology optimization for the hydrodynamic and convective heat transfer, *Commun. Nonlinear Sci. Numer. Simul.*, **131** (2024), 107819.
  - [45] J. Yang, J. Wang, and J. Kim, Energy-stable method for the Cahn-Hilliard equation in arbitrary domains, *Int. J. Mech. Sci.*, **228** (2022), 107489.